Stress-induced competing ferromagnetic and antiferromagnetic orders in epitaxial films of A-type antiferromagnet $La_{0.45}Sr_{0.55}MnO_3$

2007 J. Phys.: Condens. Matter 19 226204

(http://iopscience.iop.org/0953-8984/19/22/226204)

IOP PUBLISHING JOURNAL OF PHYSICS: CONDENSED MATTER

J. Phys.: Condens. Matter **19** (2007) 226204 (14pp) doi:10.1088/0953-8984/19/22/226204

Stress-induced competing ferromagnetic and antiferromagnetic orders in epitaxial films of A-type antiferromagnet $La_{0.45}Sr_{0.55}MnO_3$

P K Muduli, S K Bose and R C Budhani

Condensed Matter—Low Dimensional Systems Laboratory, Department of Physics, Indian Institute of Technology Kanpur, Kanpur-208016, India

E-mail: rcb@iitk.ac.in

Received 24 March 2007, in final form 16 April 2007
Published 3 May 2007
Online at stacks.iop.org/JPhysCM/19/226204

Abstract

Thin films of $La_{0.45}Sr_{0.55}MnO_3$ grown epitaxially on single-crystal surfaces which offer a tensile lattice mismatch ϵ of 1.7% and 0.47% show properties similar to that of bulk $La_{0.45}Sr_{0.55}MnO_3$ and $Nd_{0.45}Sr_{0.55}MnO_3$ respectively. These results establish a direct correlation between a reduction in lattice expansion and contraction of the lattice by the smaller rare earth ion (Nd). The antiferromagnetic-to-ferromagnetic transition in films with the lower ϵ shifts to higher temperatures as the strain is relieved with increasing film thickness. The electrical resistivity of these films at $T > T_N$ has distinct signatures of polaronic transport whose activation energy drops from ∼43 to ∼31 meV on releasing the in-plane strain. The polaron activation energy is higher by a factor of two in films of similar thickness grown on the substrate which offers the larger tensile mismatch. These results show a direct correlation between polaron binding energy (E_0) and the lattice strain. The release of strain manifested by lengthening of the out-of-plane lattice parameter also makes the Néel state robust. However, an external magnetic field (H) suppresses T_N. The resistivity of the sample at this magnetic transition shows a large negative magneto-resistance and a re-entrant metallic state at $T > T_N$ in large fields (⩾3 T). The drop in polaron activation energy seen with increasing field ($dE_0/dH \sim -3.82$ meV T^{-1}) suggests a magnetic character of the polarons. The metallic antiferromagnetic state realized in epitaxial thin films of $La_{0.45}Sr_{0.55}MnO_3$ makes it a candidate material for exchange biasing of the manganite-based magnetic tunnel junctions.

1. Introduction

The manganese oxide based perovskites, known also as manganites, show extraordinary structural, magnetic and magneto-transport properties [1–5]. One of the most widely studied

manganites, $La_{1-x}Sr_xMnO_3$, is a canonical double-exchange ferromagnet for $0.18 \leqslant x \leqslant 0.5$. While extensive literature exists on the electronic and magnetic properties of this transition metal oxide in the doping range $0 \leqslant x \leqslant 0.5$, many fascinating aspects of its overdoped regime ($x > 0.5$) still need to be addressed. This is particularly true for epitaxial films where the substrate-induced strain can affect the Mn–O–Mn overlap integral and lead to new effects in transport and magnetic properties [6–11]. Two interesting examples of manganites where subtle changes in the overlap integral result in new magnetic phases in the overdoped regime are $La_{0.45}Sr_{0.55}MnO_3$ (LSMO) and $Nd_{0.45}Sr_{0.55}MnO_3$ (NSMO) [12–18]. The ground state of LSMO is antiferromagnetic with A-type spin structure in which ferromagnetically coupled Mn–O–Mn layers (*ac*-plane) are stacked antiferromagnetically along the *b*-axis of the monoclinic structure [13–15]. This A-type antiferromagnetic ground state without charge ordering, in which the spins within the FM layers are aligned in the [101] direction, is a result of the compromise between the double-exchange interaction and a super-exchange interaction. The $d_{x^2-y^2}$ orbitals are ordered in the *ac*-plane to maximize the carrier kinetic energy via Mn^{3+}–O–Mn^{4+} double-exchange interaction and the t_{2g} local spins are coupled antiferromagnetically along the *b*-axis to gain super-exchange energy. A similar A-type antiferromagnetic ground state accompanying $d_{x^2-y^2}$ orbital ordering has also been seen in NSMO [14–17]. The A-type AFM ground state of these systems optimizes the metallic condition in the *ac*-plane, whereas the transport is thermally activated along the *b*-axis. This similarity between NSMO and LSMO ends above the Néel temperature T_N. While NSMO undergoes a first-order phase transition from the antiferromagnetic to paramagnetic state at $T_N \approx 220$ K, in LSMO the transition is from the AFM to FM state, which eventually loses spin order at $T_C \approx 300$ K. The LSMO at $T > T_C$ and the NSMO at $T > T_N$ are both tetragonal with $Pbnm$ symmetry [$a = c \leqslant b/\sqrt{2}$] [14, 16]. The magnetic state of LSMO between T_C and T_N has the propensity to phase separate, because the FM phase exists over a narrow temperature interval (T_C–$T_N \approx 80$ K) [19]. The temperature range of the FM order can be shrunk further by replacing some of the La sites with Nd [15], which causes a marginal reduction in the one-electron bandwidth due to the smaller ionic radius of the latter. The stability of this precarious FM state and the pseudo-two-dimensional metallic character of the AFM state in LSMO are also expected to be sensitive to growth-related stress in epitaxial thin films. A dramatic effect of epitaxial strain on superconducting [21] and magnetic ordering [6–11, 20] temperatures of the hole-doped Mott insulators have been reported in the literature. The AFM state in epitaxial films of $La_{0.45}Sr_{0.55}MnO_3$ is also technologically important. Such films can be used for exchange biasing of less-than-half-filled ferromagnetic LSMO, such as $La_{0.67}Sr_{0.33}MnO_3$ layers in a thin-film magnetic tunnel junction [22].

In order to investigate the role of epitaxial strain on magnetic ordering and charge transport in LSMO, we have synthesized epitaxial films of this overdoped manganite on (100) $SrTiO_3$ (STO) and (110) $NdGaO_3$ (NGO) single-crystal substrates. The films on STO are found to be under a larger tensile strain compared to the films on NGO. The magnetic ground state of both types of sample is antiferromagnetic, as indicated by a sharp cusp in magnetization at $T \approx 220$ K, but their electrical behaviours have some remarkable differences. While the films on NGO undergo a sharp metal-to-insulator [MI] transition from the metallic AFM state to the insulating PM state at $T = T_N$, the films on STO remain metallic well above T_N without any distinct changes in the resistivity near T_N. These samples eventually undergo an M–I transition at $T_{MI} \approx 300$ K. A careful measurement of magnetization between T_N and T_{MI} on these films indicates the presence of ferromagnetic fluctuations, which presumably provide channels for metallic conductivity at temperatures well beyond T_N.

2. Experiment

Thin epitaxial films of LSMO were deposited on (100) STO and (110) NGO substrates by ablating a well-sintered target of the desired stoichiometric composition, $La_{0.45}Sr_{0.55}MnO_3$, with a pulsed excimer laser (KrF, $\lambda = 248$ nm). The films were deposited at 800 °C in oxygen pressure of 300 mTorr. A growth rate of ∼1.1 Å s^{-1} was realized by firing the laser at 10 Hz with an areal energy density of ∼1.9 J cm^{-2} onto the target. The film deposition rate per laser pulse at a given energy density and substrate-to-target distance was calibrated by measuring the thickness (d_f) of several films. The deposition chamber was backfilled with O_2 to atmospheric pressure after completion of film growth and the samples were cooled to room temperature at a rate of 10 °C min^{-1}. The crystallographic structure of the films was examined with a θ–ω diffractometer (Seifert model XRD-300-P) equipped with a Cu Kα source using θ–2θ diffraction mode. For electrical measurements, silver pads were evaporated onto 2.5 × 10 mm^2 films through a shadow mask. Resistivity measurements were carried out in a liquid helium storage dewar with a dip-stick probe. The four-probe method was used for resistivity measurements in constant-current mode using a precision programmable dc current source (Keithley 224), a Lakeshore 311 temperature controller used in conjunction with a cernox sensor, and a nanovoltmeter (HP 34420 A nanovolt/micro-ohm meter). The magneto-resistance measurements were performed in a 4 T superconducting solenoid. For the measurements of magnetization, we used a superconducting quantum interference device (SQUID) based magnetometer (Quantum Design MPMS-XL5).

3. Results and discussion

3.1. Out-of-plane lattice parameter and epitaxial strain

Figures 1(a) and (b), show the θ–2θ diffraction scans taken on 1000 Å thick LSMO films deposited on (100) STO and (110) NGO substrates, respectively. The presence of only (00l) reflections in the diffraction patterns in close proximity to the (00l) reflections from the substrate indicates c-axis oriented epitaxial growth of the films. The bulk LSMO at $T \geqslant 220$ K has a tetragonal structure ($c \approx 3.87$ Å, $a = b \approx 3.84$ Å) in pseudo-cubic notation. The c-axis becomes the direction of the AFM propagation vector at $T < T_N$ [13, 14]. The lattice parameter of the substrates taken from the standard powder diffraction file (PDF)[1] and the c-axis parameter of ∼1000 Å-thick LSMO film are listed in table 1. These data show unequivocally a contraction of the c-axis of the LSMO film on STO (cubic) which has a larger lattice parameter ($a_{STO} = 3.905$ Å) compared to the in-plane lattice parameter of NGO (≃3.858 Å). It is quite natural for this to occur, as a larger in-plane lattice parameter of the substrate leads to expansion of the *ab*-plane and contraction along the growth direction of the epitaxial film. Although the in-plane lattice parameter of NGO is smaller than that of STO, it is still larger than the *ab*-plane lattice parameters of the bulk LSMO. The epitaxial strain parameter ϵ, defined as $\epsilon = (d_{bulk} - d_{sub})/d_{bulk}$, where d_{bulk} and d_{sub} are the in-plane lattice parameters of the bulk LSMO and the substrate respectively, is −1.7% for STO and −0.47% for NGO substrates. Thus, in both the cases the film in the initial stages of growth will be under a tensile strain, although the effect is smaller for the NGO substrate. The variation in the c-axis lattice parameter of the LSMO films grown on NGO substrates as a function of thickness (d_f) is shown in the inset of figure 1(b). Its increasing behaviour with d_f is consistent with the picture of a non-zero tensile strain in the plane of the film. The c-axis lattice parameter increases towards the bulk value on the relaxation of strain in thicker films. This relaxation process

[1] Standard powder diffraction file (PDF), file no. 21-971.

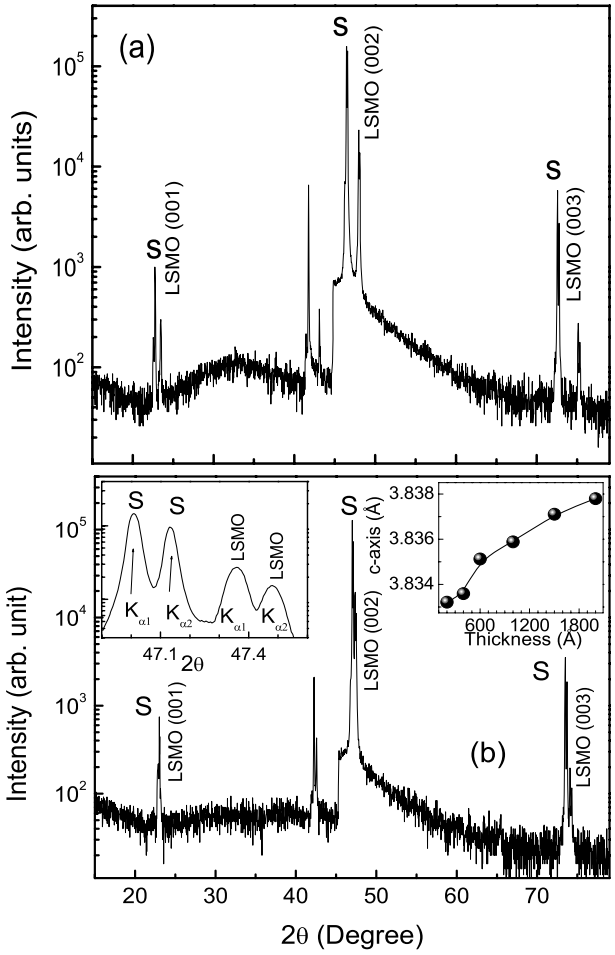

Figure 1. X-ray diffraction pattern of a 1000 Å-thick $La_{0.45}Sr_{0.55}MnO_3$ film deposited on (100) STO (a) and (110) NGO (b) substrates. The left inset of panel (b) shows the zoom-in view of the x-ray profile near the (002) peak. The variation in the *c*-axis lattice parameter with film thickness is shown in the right inset.

Table 1. The *c*-axis lattice parameter of a 1000 Å-thick $La_{0.45}Sr_{0.55}MnO_3$ film deposited on different substrates and the lattice parameter of the substrates.

Substrate	Symmetry	*a* (Å)	*c* (Å)	*c* of LSMO (Å)
$SrTiO_3$	Cubic	3.905		3.79
$NdGaO_3$	Tetragonal	3.863	3.854	3.836

begins when the film thickness exceeds ≈50 nm. Although the epitaxial strain parameter ϵ for LSMO on STO is only $\sim -1.7\%$, the tensile stress is beyond the yield strength of the film, which leads to delamination. The development of stress-induced cracks and eventual peeling of the films on STO makes measurement of electron transport and studies of the variation in lattice parameter with film thickness difficult.

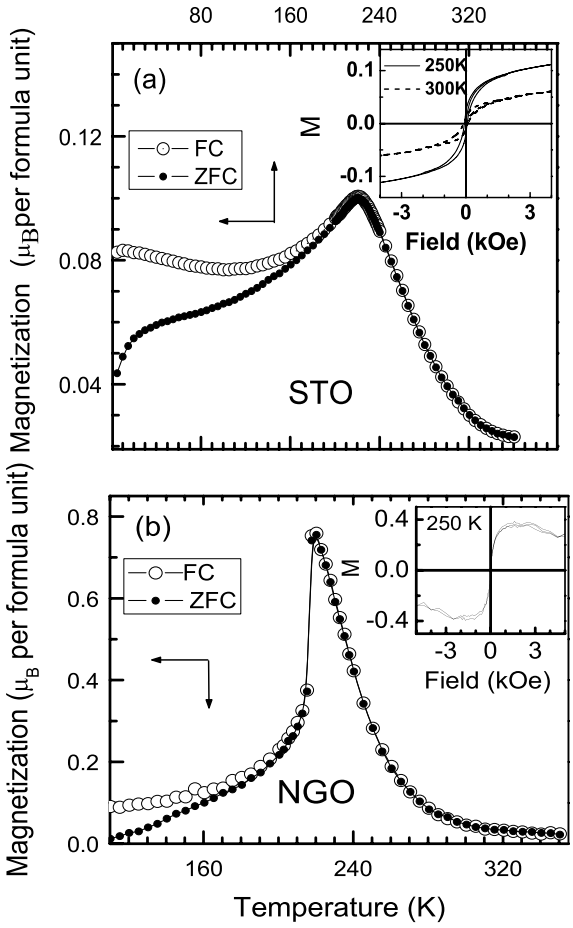

Figure 2. (a) Temperature dependence of the zero-field-cooled (ZFC) and field-cooled (FC) magnetization of a 1500 Å-thick $La_{0.45}Sr_{0.55}MnO_3$ film deposited on STO substrate. The measurement was made in a 1000 Oe in-plane field. The magnetic moment per formula unit at two temperatures, 250 and 300 K, as a function of field is shown in the inset. (b) Temperature dependence of the ZFC and FC magnetization measured in a field of 500 Oe of a 1500 Å film on NGO substrate. The inset shows the magnetic moment as a function of field applied in the plane of the film at 250 K.

3.2. Magnetic ordering

Figure 2(a) shows the temperature dependence of magnetization, $M(T)$, of a ∼1500 Å-thick film deposited on STO and measured in a 1000 Oe field applied parallel to the plane of the sample. The field-cooled (FC) and zero-field-cooled (ZFC) magnetizations rise on cooling the sample below 350 K. A cusp-like feature develops in the magnetization at ∼220 K, followed by a significant drop in the ZFC magnetization at $T < 220$ K. The peak value of magnetization is only ∼0.09 μ_B per Mn ion. In analogy with the work on bulk samples of LSMO, we identify the cusp at 220 K with the Néel temperature of the sample [12–14]. In the inset of figure 2(a), the field dependence of magnetization at two temperatures (250 and 300 K) above Néel ordering is shown. The magnetic moment at these two temperatures saturates to a value of ∼0.1 μ_B and ∼0.05 μ_B, respectively, which is quite small compared to the saturation value of 3.45 μ_B when

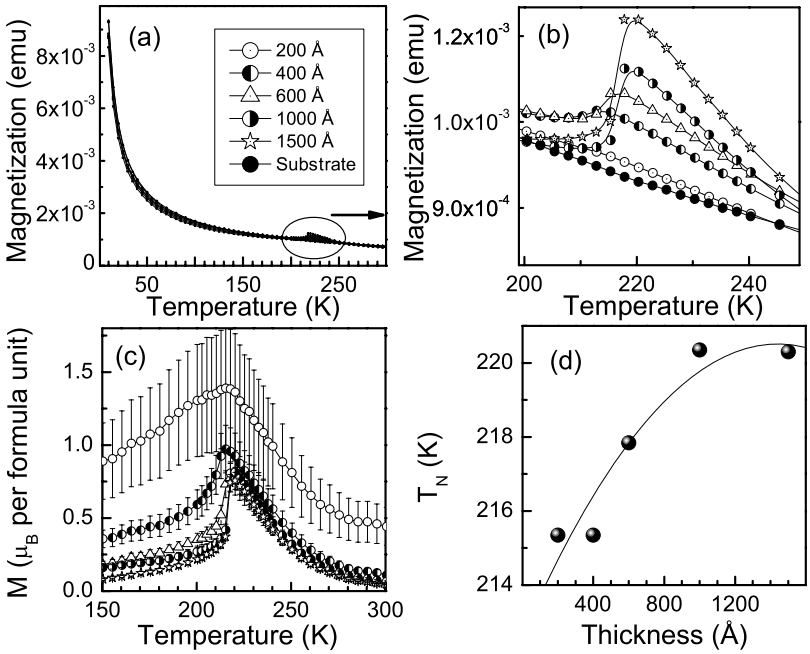

Figure 3. (a) Temperature dependence of the ZFC magnetization of $La_{0.45}Sr_{0.55}MnO_3$ films of different thickness deposited on 5×5 mm^2 (110) NGO. (b) The zoom-in view of the magnetization curves of panel (a). (c) Magnetization after correcting for the substrate contribution. Data below 150 K are not shown due to large errors in the correction. The maximum error in the value of the magnetization due to the error in the measurement of film volume is $\sim \pm 29.4\%$ (for 200 Å film). (d) Thickness dependence of the Néel temperature (T_N).

moments on all Mn^{3+} and Mn^{4+} sites in the sample would be aligned in the same direction. This minuscule ordered moment drops rapidly as the temperature approaches 300 K. The clear observation of hysteresis in the M–H data at $T > T_N$, however, suggests ferromagnetically ordered entities in the sample, which could result from nucleation of FM clusters from the Néel state. The number density of such clusters must be very small. Otherwise the saturation moment would not be significantly lower than the fully ordered value (3.45 μ_B per formula unit).

In figure 2(b) we show the temperature dependence of magnetization of a 1500 Å-thick film deposited on the NGO substrate. As NGO is strongly paramagnetic at low temperatures, the temperature dependence of magnetization is not shown below 100 K due to the difficulty in correcting for the substrate moment. Even at $T > 100$ K, the absolute error in the measurement of the moment is quite large due to the contribution of the substrate. However, the antiferromagnetic transition at $\sim$220 K can be seen as a sharp cusp in the M versus T curve. In the inset of figure 2(b) we show the field dependence of magnetization at 250 K. The strong nonlinearity of M on H at low fields ($\leqslant$1500 Oe) suggests the presence of ferromagnetic spin fluctuations in the material at $T > T_N$.

We have measured the thickness dependence of the Néel temperature of the films deposited on NGO substrates. However, as stated earlier, a careful correction for the paramagnetic contribution from the substrate needs to be carried out in order to extract the absolute value of magnetization. Figure 3(a) shows the temperature dependence of the ZFC in-plane magnetization for films of various thicknesses grown on substrates of size 5×5 mm^2. No

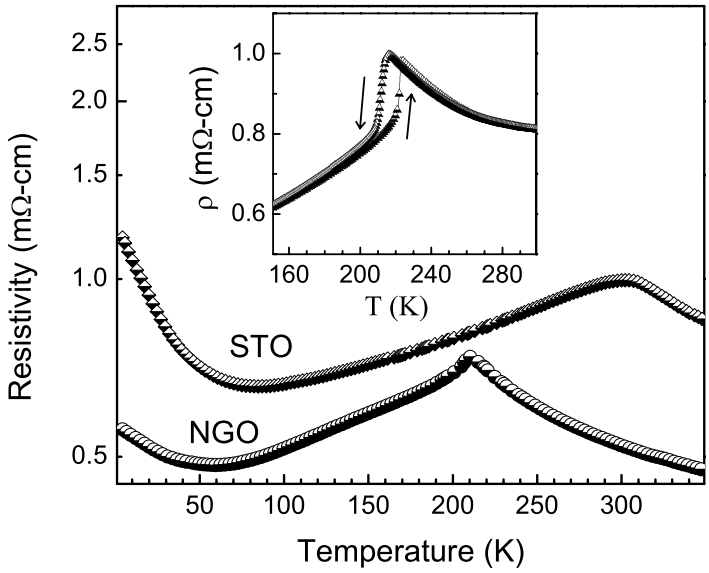

Figure 4. Temperature dependence of electrical resistivity of 200 Å thick $La_{0.45}Sr_{0.55}MnO_3$ film deposited on STO and NGO substrate. The thermal hysteresis in the resistivity of a 1000 Å thick $La_{0.45}Sr_{0.55}MnO_3$ film on NGO is shown in the inset.

substrate correction has been applied in this case. Figure 3(b) shows a zoom-in view of the same data near the Néel temperature. The magnetization after subtracting the contribution per gram of the substrate, and assuming that the mass of the film is negligible compared to the mass of the substrate, is shown in figure 3(c). Although the absolute value of magnetization still has a large error, primarily due to the uncertainty in the measurement of film volume, the position of the Néel temperature is seen clearly as a cusp whose sharpness decreases as the films are made thinner. Figure 3(d) shows the thickness dependence of T_N. The increase in T_N with film thickness can be correlated with the thickness dependence of the c-axis lattice parameter shown in the inset of figure 1(b), which also increases with d_f. The larger c-axis parameter at higher film thicknesses results in the reduction of the Mn–O–Mn double-exchange interaction along the c-axis. This strengthens the competing antiferromagnetic super-exchange between the t_{2g} spins, thereby raising the Néel temperature.

3.3. Electrical resistivity and magneto-resistance

In figure 4 we compare the temperature dependence of electrical resistivity, $\rho(T)$, of ∼200 Å-thick LSMO films deposited on STO and NGO substrates. The resistivity in both cases first drops on increasing the temperature from 4.2 K, reaches a minimum, and then follows a metallic behaviour. The low-temperature insulating state is much more pronounced in the case of the films deposited on STO. These films also have an overall higher resistivity compared to those on NGO. Since the strain parameter $|\epsilon|$ is larger for STO, a correlation between strain and resistivity and its temperature dependence are expected. The increase in resistivity below 50 K in figure 4 has been reported for other quasi-two-dimensional metallic manganites like $Nd_{0.45}Sr_{0.55}MnO_3$ [17]. The metallic behaviour seen in the intermediate-temperature regime is suppressed in a striking manner at still higher temperatures. The resistivity of the films on NGO shows a sharp cusp at ∼220 K, followed by a drop on increasing the temperature

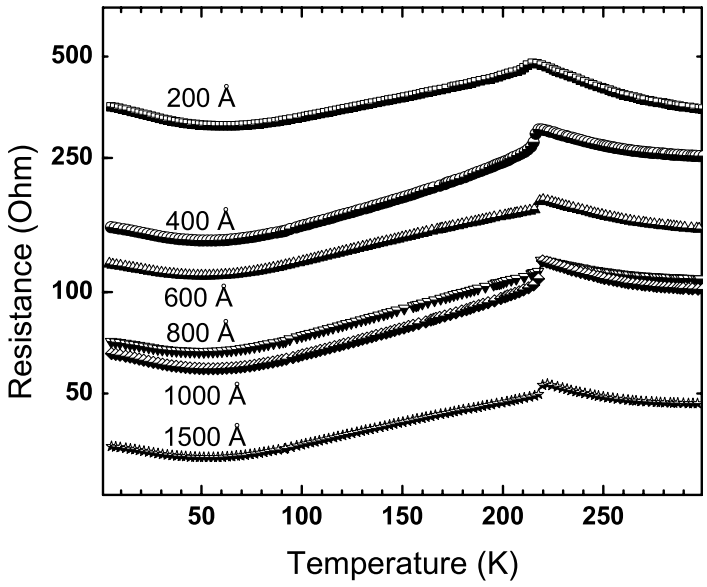

Figure 5. Temperature dependence of electrical resistance of $La_{0.45}Sr_{0.55}MnO_3$ films of thicknesses ranging from 200 Å to 1500 Å deposited on (110) NGO.

further. The cusp in resistivity occurs at the same temperature as the cusp in magnetization (see figures 2 and 3). In the inset of figure 4 we show the thermal hysteresis in resistivity in the vicinity of T_N for a 1000 Å-thick film on NGO. This highly pronounced irreversibility of $\rho(T)$ results due to a lower insulator-to-metal transition on cooling and a higher metal-to-insulator transition on warming the sample. This hysteresis in $\rho(T)$ is a signature of the first-order phase transition from the cubic PM phase to the A-type AFM state, which is a two-dimensional metal due to the in-plane double exchange. Surprisingly however, the resistivity of the film on STO deposited in the same PLD run continues to stay metallic well beyond the Néel temperature seen in the magnetization measurements (figure 2(a)) without any change in slope, $d\rho/dT$, in the vicinity of T_N. Finally, at $T \sim 300$ K ($> T_N$), the resistivity goes through a maximum and then decreases on a further increase in temperature. Note that the magnetization of these films in the vicinity of 300 K shows a rapid drop with increasing temperature (figure 2(a)). These general features of $\rho(T)$ of the films on STO are retained as the film thickness is increased to ∼500 Å. Thicker films on STO, however, develop stress-induced cracks which lead to erroneous $\rho(T)$ behaviour. The monotonic behaviour of $\rho(T)$ in the vicinity of the magnetic ordering temperature (T_N) in LSMO films deposited on (001)STO has also been reported by Izumi and coworkers [23] and Horiba *et al* [24].

We now investigate the behaviour of the in-plane resistivity $\rho(T)$ of the films deposited on NGO in some detail. Figure 5 shows the temperature dependence of resistance $R(T)$ of several films of thicknesses ranging from 200 to 1500 Å. The data for $R(T)$ instead of $\rho(T)$ are shown for the sake of clarity, because the variation in $\rho(T)$ with film thickness is within the accuracy of our measurements. While the general features of the R versus T plots are similar for all films, the cusp at T_N becomes sharper in the thicker films. The variation in the Néel temperature and the absolute resistivity at 300 K with film thickness is shown in the inset of figure 6. The T_N increases in a non-monotonic manner with film thickness and has a tendency to saturate as d_f approaches ∼1500 Å. The resistivity at 300 K on the other hand

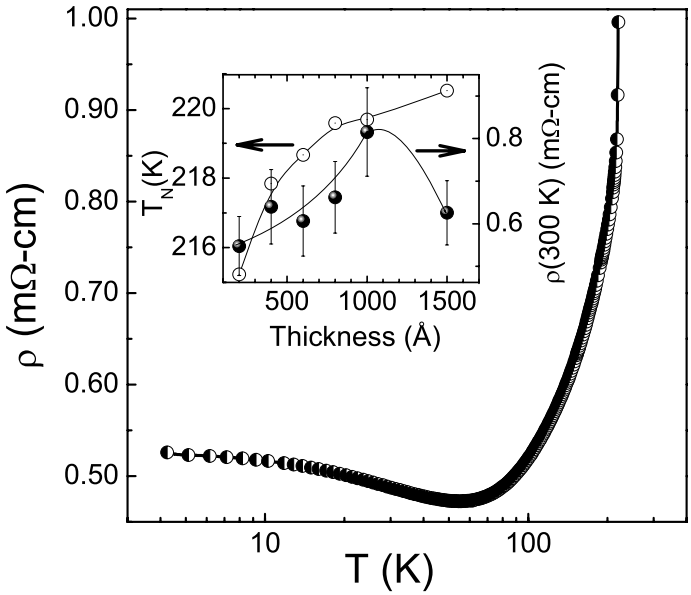

Figure 6. Temperature dependence of electrical resistivity between 5 and 220 K of a 1000 Å-thick $La_{0.45}Sr_{0.55}MnO_3$ film deposited on NGO substrate. The inset shows the variation in the Néel temperature deduced from resistivity measurements and the room-temperature resistivity, ρ (300 K), as a function of temperature.

appears to increase with d_f initially and then to decrease as the Néel temperature attains the saturation value. The large error in the measurement of ρ due to the uncertainty in sample dimensions, however, makes this result inconclusive. The main panel of figure 6 presents the typical low-temperature behaviour of the resistivity in these films. The $\rho(T)$ goes through a minimum, followed by an ln T divergence and then saturation at the lowest temperatures. This Kondo-like behaviour of the resistivity [25, 26] seen in samples of all thicknesses is somewhat surprising in a system where the transport is in planes where the t_{2g} spins of Mn ions are aligned ferromagnetically[2].

The origin of the insulator-like resistivity above the magnetic ordering temperature (T_C) seen in most of the hole-doped manganite has been a topic of considerable discussion [1, 3, 27–29]. A comparison of the thermopower and resistivity in clean samples suggests that the activated behaviour of $\rho(T)$ is due to a strong electron–lattice coupling induced localization of charge carriers into small polarons [1, 30]. Since the spin of these self-trapped carriers is strongly Hund-coupled to the local t_{2g} spin, the small polaron is also dressed with a magnetic cloud. In the adiabatic limit where the hopping frequency of the polaron is higher than the rate at which lattice distortion recovers as the charge moves away, the resistivity is given as [1, 3]

$$\rho(T) = \frac{\rho_0 T}{T_0} \exp\left[\frac{E_o}{k_B T}\right] \tag{1}$$

where the activation energy is a sum of the transfer integral I between two hopping sites, half of the polaron formation energy W_H and the band energy ϵ_0. In the non-adiabatic case, the prefactor in equation (1) changes to $\rho_0(T/T_0)^\beta$, with $\beta \approx 3/2$. We have analysed the $T > T_N$

[2] The low-temperature resistivity minimum in samples of various thicknesses is being examined in detail and the results of these studies will be published in the future.

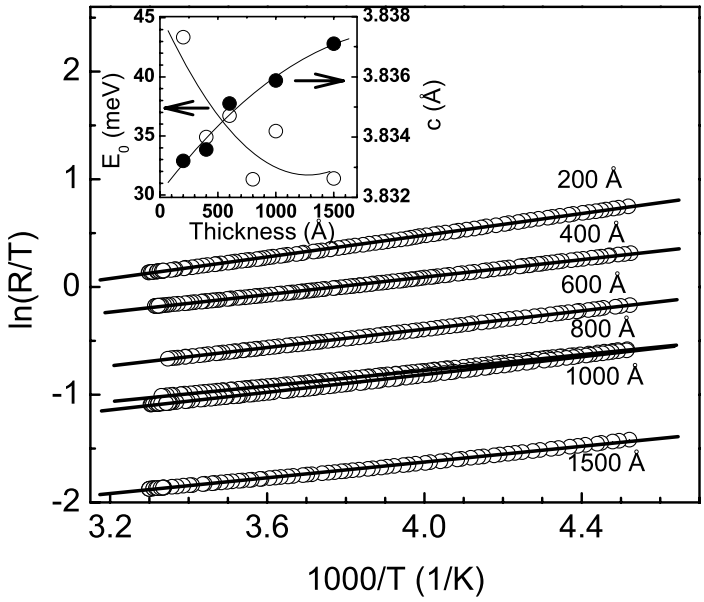

Figure 7. Temperature dependance of electrical resistivity at $T > T_N$ plotted in the framework of the adiabatic hopping of small polarons (see text). Inset shows the variation in polaron activation energy and the *c*-axis lattice parameter as a function of thickness.

resistivity of several films in the framework of the adiabatic and non-adiabatic polaron model, and the standard models of resistivity for a band-to-band excitation process which yields an Arrhenius-type temperature dependence and the variable range hopping of carriers in localized states near the Fermi energy [31]. The polaronic model yields satisfactory results, as shown in figure 7, taking $\beta = 1$ (adiabatic case) for films of different thicknesses deposited on NGO substrate. We note that these data fit equally well within the accuracy of our measurements for $\beta = 3/2$. The activation energy E_0 extracted from the fit is 43.36 meV (for $\beta = 1$) for the 200 Å-thick film. It is reduced by ≈27% as the film thickness changes from 200 to 1500 Å. The thickness dependence of E_0 is shown in the inset of figure 7. Here we also reproduce the *c*-axis lattice parameter data of figure 1. The polaron model of resistivity holds in the case of the films on STO as well at $T > T_C$. The activation energy for the 200 Å film is ≈65.56 meV. From a comparison of the hopping energy with film thickness and *c*-axis lattice parameter, which increases as the epitaxial strain is released in thicker films, it is clear that the strain makes the hopping of polarons difficult. This conclusion is also supported by the large value of E_0 in the 200 Å-thick film deposited on STO, where the in-plane tensile strain is much greater. From these studies we conclude that, while the resistivity and magnetization of the films on STO compare well with data on bulk crystals of $La_{0.45}Sr_{0.55}MnO_3$ [15], the thin films on NGO mimic the behaviour of $Nd_{0.45}Sr_{0.55}MnO_3$ single crystals [17]. Since Nd^{3+} is a smaller ion than La^{3+}, the bandwidth available to the e_g electron is reduced in $Nd_{0.45}Sr_{0.55}MnO_3$, which in turn completely suppresses the intermediate FM state seen in the larger-bandwidth compound $La_{0.45}Sr_{0.55}MnO_3$. Our result on LSMO films deposited on STO and NGO thus indicate that the epitaxial strain is complementary to the ionic-size-induced chemical pressure. The large tensile strain in the films on STO promotes the stability of the FM phase, whereas a reduced strain on NGO suppresses this intermediate phase.

In figure 8 we show the temperature dependence of the electrical resistivity of a 1000 Å-thick LSMO film deposited on NGO. The measurements have been performed at several values

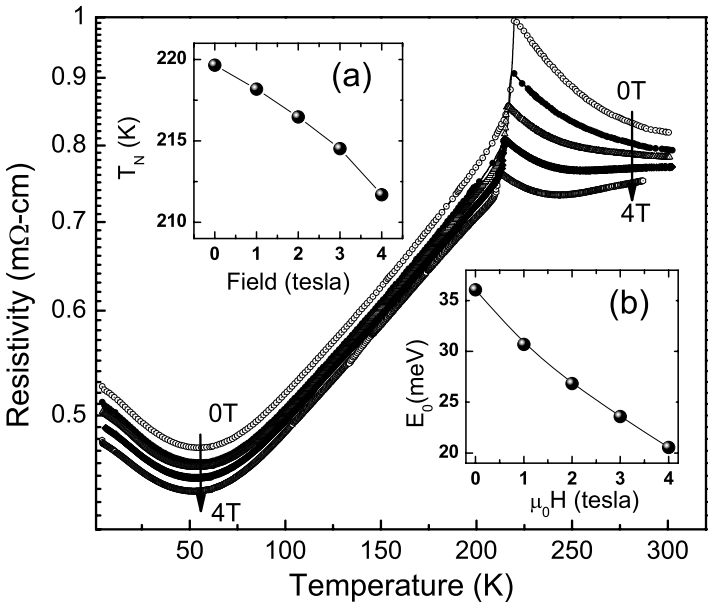

Figure 8. Temperature dependence of the electrical resistivity of a 1000 Å-thick $La_{0.45}Sr_{0.55}MnO_3$ film in the presence of a magnetic field applied parallel to the plane of the NGO substrate. The field dependences of the Néel temperature and activation energy E_0 are shown in the insets (a) and (b), respectively.

of dc field applied in the plane of the film along the direction of the current. It can be seen that the peak in resistivity at T_N is suppressed strongly by the field. While a similar suppression of the resistivity at T_C occurs in less-than-half-filled double-exchange manganites such as $La_{0.67}Ca_{0.33}MnO_3$, the shift of the peak in the present case is towards the lower temperatures. In double-exchange ferromagnets, the peak in resistivity shifts to higher temperatures due to the field-assisted ferromagnetic correlations, which widen the metallic regime. The inset (a) of figure 8 shows the variation in T_N with magnetic field. The trend seen in the inset is an indication of how the external field can suppress the onset of Néel order. The effect of magnetic field on resistivity has two regimes of behaviour in temperature here. In the temperature range of 4.2 K to T_N (∼220 K), the resistivity drops linearly with field and the $d\rho/dH$ is small ($\sim -11.7\ \mu\Omega$ cm T^{-1} at $T = 4.2$ K). However, at $T > T_N$ a large drop in resistivity is seen. In fact, as the field increases to 4 T, there is a re-entrant behaviour where the metallic regime is revisited at $T > T_N$. This is seen clearly in the Arrhenius plot of figure 9, where the zero and 4 T field resistivity at $T > T_N$ is displayed. This figure also shows that a single activation energy picture is not appropriate to explain the behaviour of the resistivity. However, the data are in good agreement with the polaron model. The drop in polaron hopping energy with field, as seen in the inset (b) of figure 8, can be attributed to them being dressed with a magnetic cloud. The presence of magnetic polarons in the paramagnetic (PM) state of manganites has been established by small-angle inelastic neutron scattering by de Teresa *et al* [32]. Jakob *et al* [33] have expressed the magnetic-field-dependent activation energy for small polaron transport as $E_0 = E_0^0(1 - \langle\cos\theta_{IP}\rangle)$, where θ_{IP} is the angle between the moment of the polaron and the angle of the moment at the ionic site to which the polaron hops. The external field lines up the two moments, resulting in a decrease in the activation energy. However, alternative proposals also exist for the drop in the activation energy with field in the PM state. Viret *et al* [34]

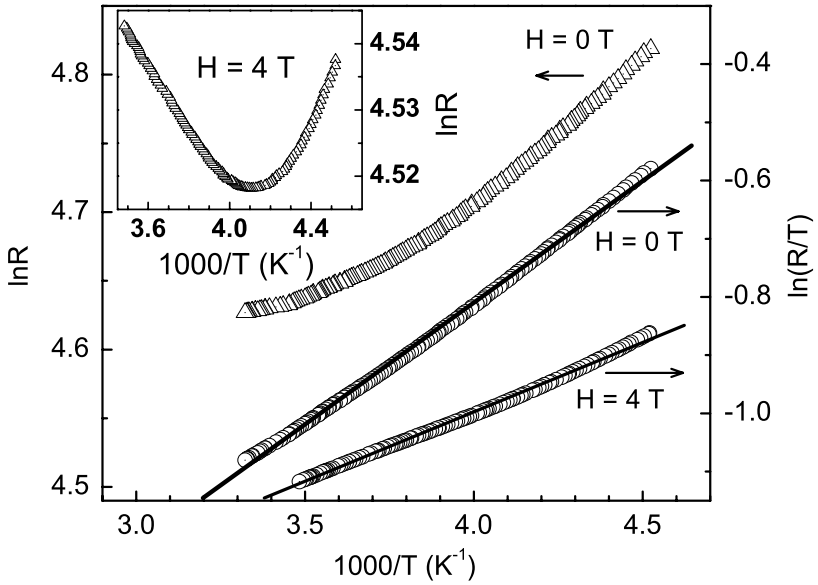

Figure 9. Electrical resistance of a 1000 Å-thick film in zero field and in a 4 T in-plane field plotted as a function of temperature to highlight the applicability of a particular model for thermally activated transport (see text). The inset shows the 4 T data plotted to highlight the re-entrant metallic behaviour at $T > T_N$ in the presence of a strong magnetic field.

argued that in the paramagnetic state the e_g electrons are localized by a random spin-dependent potential which makes the transport of variable-range-hopping (VRH) type. While the spin-dependent VRH picture is consistent with the resistivity of several less-than-half-filled double-exchange manganites, this model of transport is not consistent with the data in the present case (figure 9). Ramakrishnan *et al* [29] have considered the splitting of the two-fold-degenerate e_g band in doped manganites into a polaronic component and a band of extended states. They envisage that electrical conduction at $T > T_C$ in the less-than-half-filled double-exchange systems is due to thermal excitation of these electrons across a small gap which opens up at $T \approx T_C$. The present results seem to suggest that in the $x > 0.5$ system the motion of polarons is the dominant mechanism of transport. The same also holds in epitaxial films of $x < 0.5$ manganites [30, 33, 35] where the lattice strain can trap the broad-band states envisaged in [30].

4. Summary

In summary, we have investigated the effect of epitaxial strain on the magnetic and transport properties of $La_{0.45}Sr_{0.55}MnO_3$ thin films. Two different substrates, (001) STO and (110) NGO, were used to impart a different degree of tensile strain in the films. The magnetization of the LSMO films deposited on both types of substrates shows the onset of Néel order at ≈220 K. While the electrical resistivity of films deposited on NGO also displays a concomitant insulator-to-metal transition on cooling through T_N, the $\rho(T)$ of the highly strained films on STO is remarkably different. These films are metallic above as well as below T_N with a continuous $d\rho(T)/dT$ at T_N. We attribute the metallic state at $T > T_N$ to ferromagnetic correlations which appear in a phase-separated manner and provide conducting channels in the sample. These correlations disappear at a well-defined temperature T_C (≈ 300 K) above which the resistivity is thermally activated. A comparison of the magnetic ordering and $\rho(T)$ of these films with

bulk samples of $La_{0.45}Sr_{0.55}MnO_3$ and $Nd_{0.45}Sr_{0.55}MnO_3$ suggests a direct correlation between epitaxial strain and chemical pressure due to substitution. An interesting correlation is also seen between the out-of-plane lattice parameter (c) and the Néel temperature. The latter rises with 'c' as the in-plane strain is relaxed with increasing film thickness. A qualitative explanation for this behaviour of T_N can be given in terms of the enhanced in-plane double-exchange interaction due to strain; the out-of-plane interaction which reduces the Mn–O–Mn bond distance then becomes dominantly antiferromagnetic due to super-exchange, which stabilizes the A-type AF state in the first place. Increasing c reduces the dipole interaction and makes the AF state more robust. T_N is suppressed by an external magnetic field, suggesting a complementary role of the dipolar coupling and that the field weakens the Néel state. The transport in the magnetically disordered state has the characteristics of magnetic polaron hopping with concomitant large negative magneto-resistance. The polaron activation energy shows a clear increase with the tensile strain in the films.

Acknowledgments

This research has been supported by the Indo-French Center for Promotion of Advanced Research, New Delhi and the internal funding of the Indian Institute of Technology, Kanpur. P K Muduli and S K Bose acknowledge financial support from the Council for Scientific and Industrial Research, Government of India. Technical assistance with SQUID measurements from Mr R Sharma is also acknowledged.

References

[1] Salamon M B and Jaime M 2001 *Rev. Mod. Phys.* **73** 583
[2] Dagotto E, Hotta T and Moreo A 2001 *Phys. Rep.* **344** 1
[3] Coey J M D, Viret M and Molnar S Von 1999 *Adv. Phys.* **48** 167
[4] Rao C N R and Raveau B 1998 *Colossal Magnetoresistance, Charge-Ordering and Related Aspects of Manganese Oxides* (Singapore: World Scientific)
[5] Tokura Y and Tomioka Y 1999 *J. Magn. Magn. Mater.* **200** 1
[6] Suzuki Y, Hawang H Y, Cheong S-W and Van Dover R B 1997 *Appl. Phys. Lett.* **71** 140
[7] Millis A J, Darling T and Migliori A 1998 *J. Appl. Phys.* **83** 1588
[8] Wu T, Ogale S B, Shinde S R, Biswas A, Polletto T, Greene R L, Venkatesan T and Millis A J 2003 *J. Appl. Phys.* **93** 5507
[9] Ogimoto Y, Nakamura M, Takuko N, Tamaru H, Izumi M and Miyano K 2005 *Phys. Rev.* B **71** R060403
[10] Ahn K H, Lookman T and Bishop A R 2004 *Nature* **428** 401
Ahn K H, Lookman T and Bishop A R 2006 *J. Appl. Phys.* **99** 08A703
[11] Konishi Y, Fang Z, Izumi M, Manako T, Kasai M, Kuwahara H, Kawasaki M, Terakura K and Tokura Y 1999 *J. Phys. Soc. Japan* **68** 3790
[12] Fujishiro H, Ikebe M and Konno Y 1998 *J. Phys. Soc. Japan* **67** 1799
[13] Joonghoe D, Kim W S and Hur N H 2001 *Phys. Rev. Lett.* **87** 187201
Joonghoe D, Chi E O, Kim W S, Hur N H and Choi Y N 2002 *Phys. Rev.* B **65** 132414
[14] Moritomo Y, Akimoto T, Nakamura A, Ohoyama K and Ohashi M 1998 *Phys. Rev.* B **58** 5544
[15] Akimoto T, Maruyama Y, Moritomo Y, Nakamura A, Hiota K, Ohoyama K and Ohashi M 1998 *Phys. Rev.* B **57** R5594
[16] Yoshizawa H, Kawano H, Fernandez-Baca J A, Kuwahara H and Tokura Y 1998 *Phys. Rev.* B **58** R571
[17] Kuwahara H, Okuda T, Tomioka Y, Asamitsu A and Tokura Y 1999 *Phys. Rev. Lett.* **82** 4316
[18] Yoshizawa H, Kajimoto R, Kawano H, Fernandez-Baca J A, Tomioka Y, Kuwahara H and Tokura Y 1999 *Mater. Sci. Eng.* B **63** 125
[19] Yoo J H, Murakami Y, Shindo D, Atou T and Kikuchi M 2002 *Phys. Rev.* B **66** 212406
[20] Rao R A, Lavric D, Nath T K, Eom C B, Wu L and Tsui F 1998 *Appl. Phys. Lett.* **73** 3294
[21] Locquet J-P, Perret J, Fompeyrine J, Mchler E, Seo J W and Van Tendeloo G 1998 *Nature* **394** 453

[22] Pailloux F, Imhoff D, Sikora T, Barthelemy A, Maurice J-L, Contour J-P, Colliex C and Fert A 2002 *Phys. Rev.* B **66** 014417
[23] Izumi M, Manako T, Konishi Y, Kawasaki M and Tokura Y 2000 *Phys. Rev.* B **61** 12187
[24] Horiba K, Chikamatsu A, Kumigashira H, Oshima M, Nakagawa N, Lippmaa M, Ono K, Kawasaki M and Koinuma H 2005 *Phys. Rev.* B **71** 155420
[25] Kondo J 1964 *Prog. Theor. Phys. (Kyto)* **32** 37
[26] Daybell M D and Steyert W A 1968 *Rev. Mod. Phys.* **40** 380
[27] Kubo K and Ohata N 1972 *J. Phys. Soc. Japan* **33** 21
[28] Millis A J, Littlewood P B and Shraima B I 1995 *Phys. Rev. Lett.* **74** 5144
[29] Ramakrishnan T V, Krishnamurthy H R, Hassan S R and Venketeswara Pai G 2004 *Phys. Rev. Lett.* **92** 157203
[30] Jaime M, Salamon M B, Pettit K, Rubinstein M, Treece R E, Horwitz J S and Chrisey D B 1996 *Appl. Phys. Lett.* **68** 1576
[31] Mott N F and Davis E A 1979 *Electronic Processes in Non-Crystalline Solids* (London: Oxford University Press)
[32] De Teresa J M, Ibarra M R, Algarabel P A, Ritter C, Marquina C, Blasco J, Garca j, del Moral A and Arnold Z 1997 *Nature* **386** 226
[33] Jakob G, Westerburg W, Martin F and Adrian H 1998 *Phys. Rev.* B **58** 14966
[34] Viret M, Ranno L and Coey J M D 1997 *Phys. Rev.* B **55** 8067
[35] Worledge D C, Jeffrey S G, Beasley M R, Geballe T H, Ron H and Steve D 1996 *J. Appl. Phys.* **80** 5158